Low-Frequency Magnetic Shielding of Double-Layer Conducting Plates with Periodic Apertures: Experimental Observation of Great Improvement of Shielding Effectiveness by Slightly Separating the Two Plates

Feiyan Zhou[1], Yan Wu[1], Lingyun Gu[1], Xuefeng Bai[1],
Yan Wu[1], Yang Wang[2], Dingyu Qin[2], and Chongqing Jiao[2, *]

Abstract—This article focuses on the low-frequency magnetic shielding of double-layer conducting plates with periodic circular apertures. The shielding effectiveness (SE) is measured as the insertion loss of the plates when they are placed between a pair of coaxial loops, one for magnetic field emission and the other for receiving. Our experimental results show that the SE sharply increases with the layer-to-layer spacing increasing from zero to the aperture diameter. For aluminum plates with 1 mm thickness, 20 mm unit cell, and 10 mm aperture diameter, the enhancement is approximately 10 dB and 20 dB for 3 mm and 9 mm spacing, respectively. In addition, the effect of the lateral deviation on the SE is evident only if the spacing is smaller than the aperture diameter.

1. INTRODUCTION

Low-frequency magnetic shielding is frequently commonly used to prevent electromagnetic interference in various practical applications, including electric vehicles [1], wireless power transfer [2, 3], power converters [4], ultrasensitive atomic sensors [5], resistance spot welding [6], magnetic resonance imaging [7], and power transformers [8]. Depending on specific requirements and working environments, different shielding configurations are selected, such as enclosures [1, 9], solid plates [10–14], perforated plates [15–17], and wire meshes [18–21]. Among these, perforated plates offer moderate shielding effectiveness (SE), ventilation capacity, and weight, making them especially suitable for situations where a tradeoff among SE, ventilation, and weight is required.

A recent study [15] examined the SE of a single-layer conducting plate with periodic apertures (CPPA) against a circular-loop electromagnetic field source, both theoretically and experimentally. The study found that magnetic diffusion and aperture leakage were the dominant effects in the low- and high-frequency ranges, respectively. As frequency increased, the SE was initially improved but eventually stabilized when the aperture leakage effect became dominant. The investigated single-layer CPPA exhibited an SE of approximately 40 dB in the frequency range from tens of 1 kHz to 1 MHz.

In [22], the SE of a multilayer metal mesh against a plane-wave source was studied, and it was found that the SE of metal meshes can be significantly improved by increasing the spacing between the mesh layers. However, the spacing considered was greater than at least two times of the size of the unit cell, which rendered the layer-to-layer coupling negligible. Consequently, each layer could be modelled independently using the surface impedance.

This article builds upon earlier research on a single-layer conducting plate with periodic apertures (CPPA) [15] by studying the SE of a double-layer CPPA. This article builds upon earlier research on a single-layer conducting plate with periodic apertures (CPPA) [15] by studying the SE of a double-layer CPPA. It should be noted that for such a small spacing, the analytical theory based on the traditional surface impedance formula is no longer applicable [15, 19, 21]. This is because the surface impedance will be affected by the close layer-to-layer coupling. Furthermore, achieving steady and reliable full-wave numerical simulations for such a configuration is also challenging. As a result, this article only presents experimental results, which may inspire future analytical and numerical simulation research on this article.

The rest of the article is organized as follows. Section 2 describe the electromagnetic problem and test bench setup. In Section 3, experimental results are presented, and the effects of layer-to-layer spacing and lateral deviation are analyzed. Furthermore, the edge effect of a finite-size plate is evaluated, and experiments are conducted with different aperture diameters. Finally, Section 4 provides a summary of the article.

2. PROBLEM DESCRIPTION AND TEST BENCH SETUP

As depicted in Fig. 1, the emitting loop lies on the $z = 0$ plane and has a radius of r_c. It carries a time-harmonic current i with frequency f. The first and second layers of the double-layer CPPA shield occupy the regions $z_1 < z < z_1 + t$ and $z_2 < z < z_2 + t$, respectively, where t is the thickness of each layer. Both layers are composed of same conductive material with conductivity σ, permeability μ, and permittivity ε. The dimensions of a unit cell of the CPPA shield are w along both the x axis and y axis. The radius of the circular apertures drilled periodically in the plate is r.
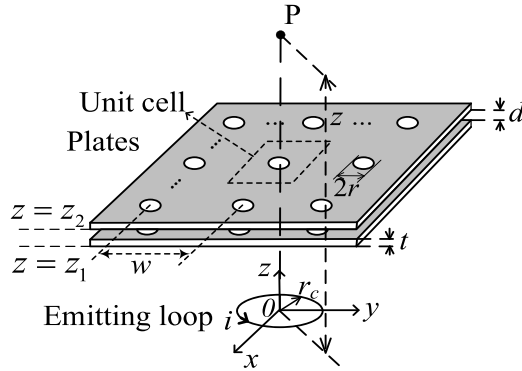
Figure 1. Sketch of the low-frequency magnetic shielding problem.

Figure 2 depicts a schematic of the test-bench setup [12], which utilized a low-frequency power signal generator (ZN1042A) to provide power to an emitting loop (ZN30303, with a diameter of 12 cm) at a frequency that could be adjusted between 1 and 500 kHz using a sine wave. The emitting loop was composed of 20 turns of enameled wire with a finite radius r_c and was fixed on a metal shell. The shell had a height of 6 cm, and the wire was fixed at a height of 5 cm above the bottom of the shell. A receiving loop (AARONIAAG, PBS-H4, with a diameter of 5 cm) was connected to a spectrum analyzer. The wire shell of the loop had a radius of 5 mm. The magnetic shielding effectiveness (SE) was determined by calculating the ratio of the voltage measured by the receiving loop with the plates removed to that with the plates loaded. Since the radius of the receiving loop was very small, the SE definition based on the induced voltage on the receiving loop was approximately equal to that based on the magnetic field at the center of the loop. Additionally, the SE could be affected by the radius of the emitting loop if the loop-to-loop distance was smaller than the loop radius [13]. The conducting plates used in the experiment had dimensions $1 \text{ m} \times 1 \text{ m} \times 1 \text{ mm}$ and were constructed of aluminum with electrical conductivity $\sigma = 3.77 \times 10^7 \text{ S/m}$ and relative permeability $\mu_r = 1$. Each aluminum plate had 2500 circular apertures of a diameter of 10 mm, and the center-to-center distance of adjacent apertures was 20 mm. z_1 is always 50 mm.
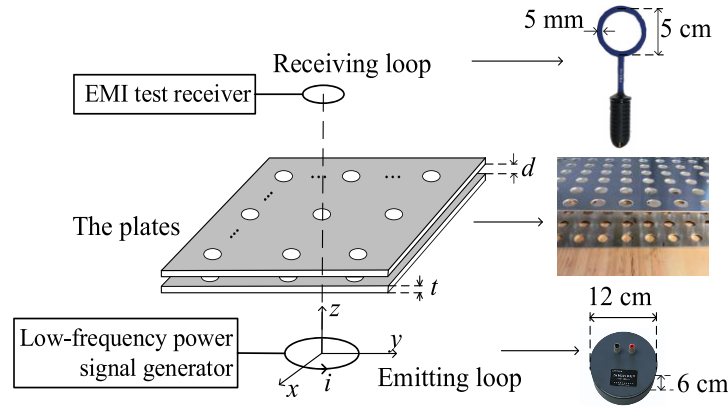
Figure 2. Test bench setup for measuring the magnetic shielding effectiveness.

3. EXPERIMENTAL RESULTS

3.1. Edge Effect

When dealing with finite-sized plates, a third coupling path, known as the edge effect, must be taken into consideration in addition to the diffusion effect and aperture leakage effect observed in infinite plates. In a study conducted by [23], the SE of a rectangular copper plate measuring $630\,\text{mm} \times 490\,\text{mm} \times 0.3\,\text{mm}$ was measured and found to be comparable to that of an infinite plate for frequencies lower than $600\,\text{kHz}$ at a loop-to-loop distance of $75\,\text{mm}$, indicating that the edge effect was negligible at these conditions. However, the extent to which the edge effect can be ignored depends on various factors such as the size of the plate, the frequency, the size of the loop, and the position of the field point. Generally, at higher frequencies, smaller plate sizes, larger loop sizes, and greater loop-to-loop distances, the edge effect will become more significant relative to the diffusion and aperture leakage effects [23].

To experimentally evaluate the edge effect, the two-layer CPPA was laterally moved while keeping the emitting and receiving loops fixed, as illustrated in Fig. 3. Fig. 4 presents the measured SE versus the lateral deviation distance. The parameters used were $f = 500\,\text{kHz}$; z_1 is always fixed at $50\,\text{mm}$; the loop-to-loop distance is $92\,\text{mm}$, and $z_2 = 51\,\text{mm}$, $57\,\text{mm}$, or $81\,\text{mm}$. It can be observed that the SE curve is stable in the middle and drops on both sides. The stable stage has a length of approximately $0.6\,\text{m}$, which is smaller than the plate length of $1\,\text{m}$. Thus, when the loops are placed within the middle region, the edge effect can be considered negligible. Conversely, if the loops are beyond the stable stage, the edge effect becomes non-negligible. Furthermore, the shielding of the edge effect becomes stronger as the layer-to-layer distance increases.
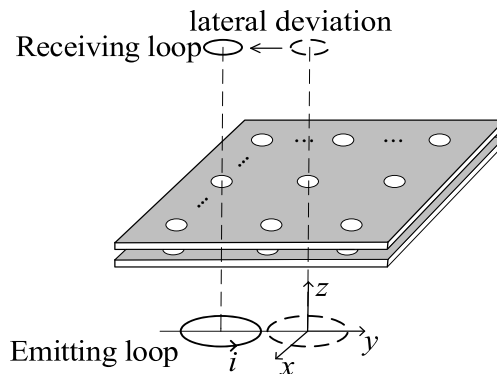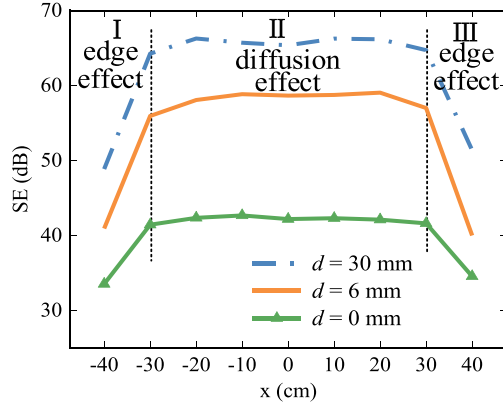

**Figure 3.** Sketch of the experiment on the edge effect.

Figure 4. Dependence of the SE on the lateral deviation of the two-layer CPPA with both the emitting and received loops fixed. The loop-to-loop distance is 92 mm, the frequency $f = 500\,\text{kHz}$, $z_1 = 50\,\text{mm}$, and $z_2 = z_1 + d + t$.

3.2. Effect of Layer-to-Layer Spacing

Here, the effect of layer-to-layer spacing on the SE is investigated, assuming that the two plates are aligned with each other. Fig. 5(a) shows the measured results for spacings of $d = 0\,\text{mm}$, $3\,\text{mm}$, $6\,\text{mm}$, $9\,\text{mm}$, and $30\,\text{mm}$, with a fixed loop-to-loop distance of 92 mm. The experimental results for a single-layer plate are also shown. As observed in the case of a single-layer plate [15], the SE initially increases with frequency and then becomes stable above some critical frequency. It is the effects of diffusion and of aperture leakage that are responsible for the magnetic field coupling mechanism respectively below and above the critical frequency. Here, we mainly focus on the aperture leakage effect, where the plates can be approximated as perfectly electric conductors. We observe a rapid increase in the SE when the two plates are slightly separated. Compared to the case of close contact ($d = 0\,\text{mm}$), the SE increments are approximately 10 dB, 18 dB, 20 dB, and 25 dB for $d = 3\,\text{mm}$, $6\,\text{mm}$, $9\,\text{mm}$, and $30\,\text{mm}$, respectively. The SE of the double-layer shield with $d = 0\,\text{mm}$ is only about 5 dB larger than that of the single-layer shield. The double-layer shield in close contact has an aperture depth of two times of that of the single-layer shield, which then causes stronger aperture attenuation based on the waveguide cutoff effect. This may be responsible for the 5 dB increment. In addition, the curve corresponding to $d = 30\,\text{mm}$ exhibits a sharp peak caused by a low-frequency resonance phenomenon. This phenomenon usually occurs when the field from the aperture leakage effect is approximately equal in magnitude to that from the diffusion effect, but is out of phase with it [24].

Figure 5(b) shows the effect of plate-to-loop spacing for a loop-to-loop distance of 77 mm. As seen
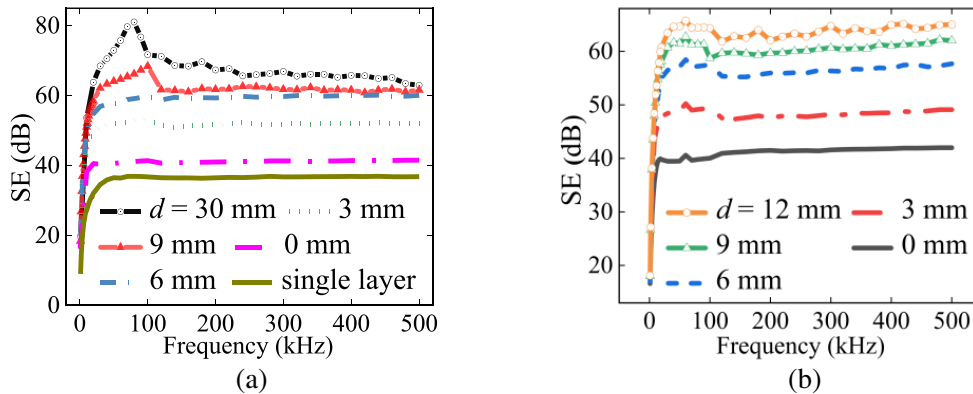
Figure 5. Measured shielding effectiveness versus frequency for different plate-to-plate spacings when the loop-to-loop distance is (a) 92 mm and (b) 77 mm. The plate thickness is 1 mm.

in the graph, the SE increases by approximately $7\,\mathrm{dB}$, $15\,\mathrm{dB}$, $19\,\mathrm{dB}$, and $23\,\mathrm{dB}$ for plate-to-loop spacings of $d = 3\,\mathrm{mm}$, $6\,\mathrm{mm}$, $9\,\mathrm{mm}$, and $12\,\mathrm{mm}$, respectively, compared to the case of close contact ($d = 0\,\mathrm{mm}$). It is worth noting that the increase in SE is relatively small with increasing distance between the emitting loop and receiving loop, as observed by comparing Figures 5(a) and 5(b).

In Figure 6, the measured SE of two plates, each of thickness $0.5\,\mathrm{mm}$ when they are naturally stacked together, is compared with that of a single plate of thickness $1\,\mathrm{mm}$ (i.e., the two stacked plates have a total thickness equal to that of the single plate). It can be seen that the two configurations have nearly identical SE, with a difference of less than $1\,\mathrm{dB}$, indicating that the influence of surface contact (pressure) between the two plates on the SE is negligible. The underlying reason for this is that in the coaxial configuration, the eddy currents within the plates have a negligible z component, and hence the eddy current loops are not cut off by the tiny gap between the plates.
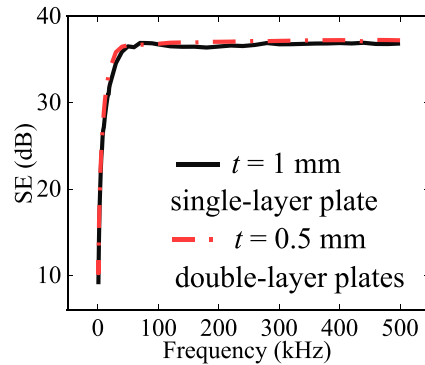
Figure 6. Comparison of the SE of a stack of two plates each of thickness $0.5\,\mathrm{mm}$ and that of a single plate of thickness $1\,\mathrm{mm}$.

3.3. Effect of Lateral Deviation

During the aforementioned tests, the two plates were always aligned. That is, one plate would completely coincide with the other after translation along the z axis. Here, we investigate the scenario where the two plates are not aligned. In particular, we let the second plate translate a distance of $w/2$ along both x and y axes simultaneously, as illustrated in Figure 7. The white circles in the figure represent the periodic apertures of the first layer, while the gray circles denote those of the second layer. In this case, the apertures of the two plates complement each other perfectly, resulting in higher SE effect than other cases of lateral deviation.
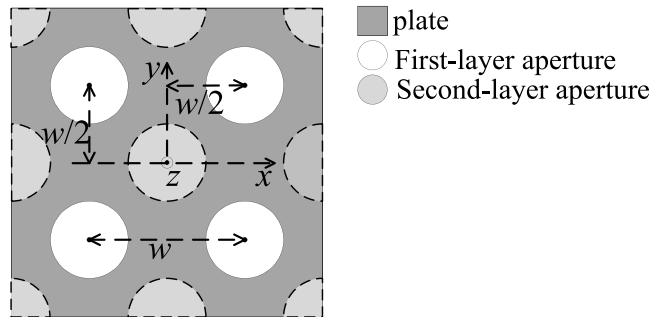
Figure 7. Top view of layer-to-layer lateral offset.

The upper limit of the loop-to-loop distance is constrained by the dynamic range of the test-bench and edge effects. And the lower limit of the distance is determined by the thickness of the emitting loop, layer-to-layer spacing, and plate thickness. Consequently, the loop-to-loop distance falls between
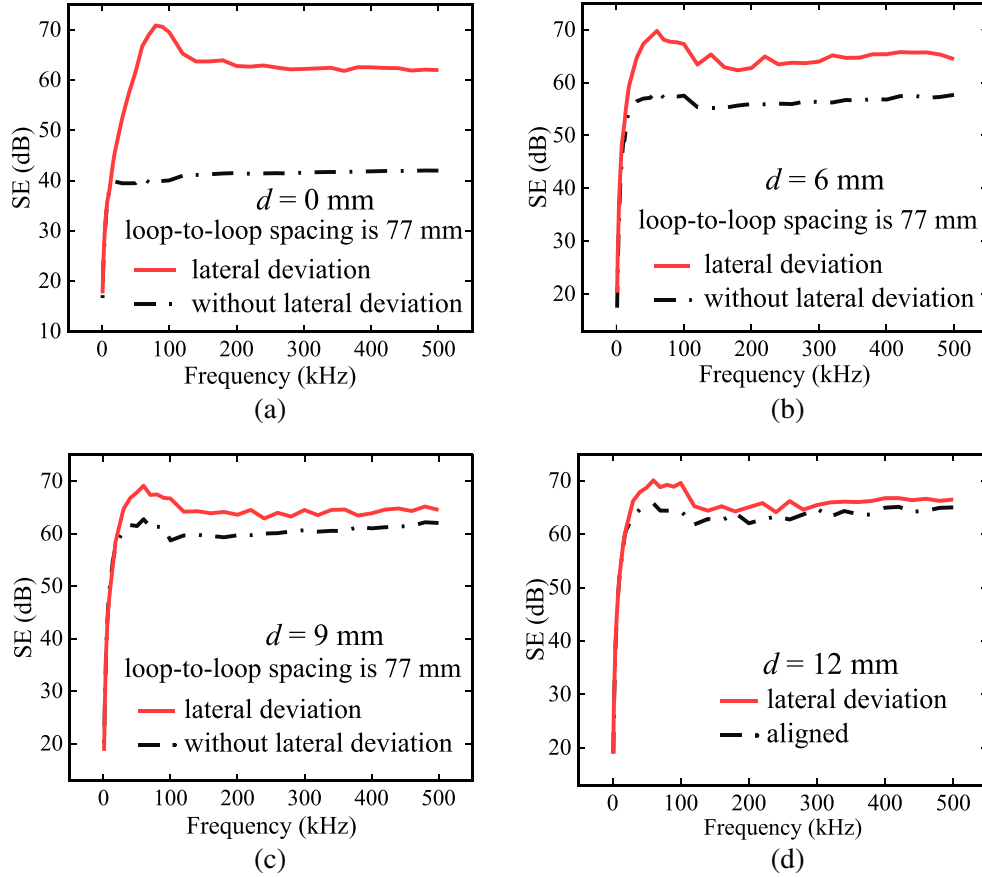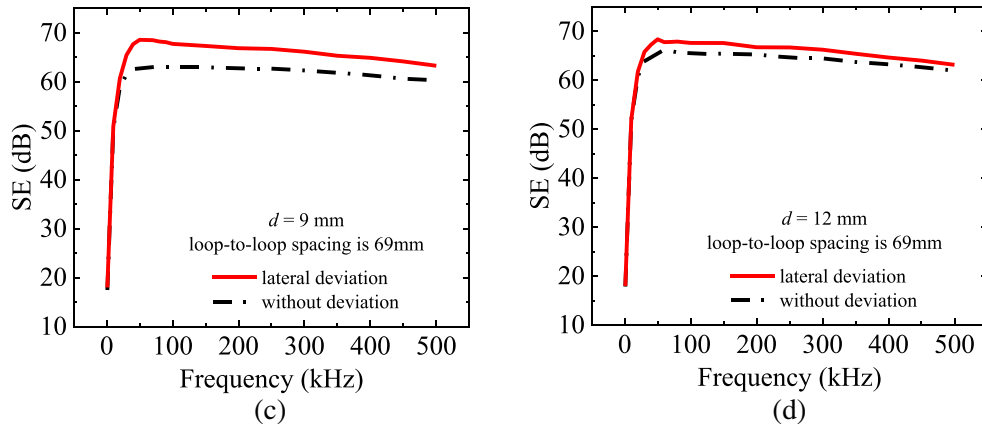
Figure 8. Comparison of SE with and without lateral deviation for a loop-to-loop distance of 77 mm with different layer-to-layer spacings: (a) $d = 0$ mm, (b) $d = 6$ mm, (c) $d = 9$ mm, and (d) $d = 12$ mm.

65 mm and 110 mm. We selected loop-to-loop distances of 69 mm, 77 mm, 92 mm, and 107 mm for our experiments. The effects of lateral deviation on the SE are shown in Figures 8–12. Specifically, Figures 8(a)–8(d) display the results for layer-to-layer distances of 0 mm, 6 mm, 9 mm, and 12 mm, respectively, with a loop-to-loop spacing of 77 mm. The results for the case with no lateral deviation are also presented for comparison.

It is apparent that lateral deviation significantly enhances the SE at smaller layer-to-layer distances. In the high-frequency region, where the aperture leakage effect is dominant, the increase in SE is approximately 21 dB, 9 dB, 4 dB, and 2 dB for $d = 0$ mm, 6 mm, 9 mm, and 12 mm, respectively.
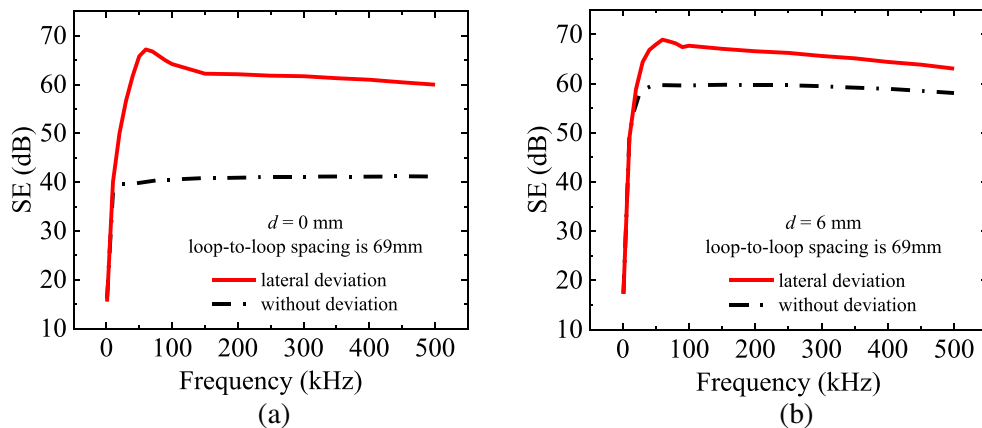
Figure 9. Comparison of SE with and without lateral deviation for a loop-to-loop distance of 69 mm with different layer-to-layer spacings: (a) $d = 0$ mm, (b) $d = 6$ mm, (c) $d = 9$ mm, and (d) $d = 12$ mm.
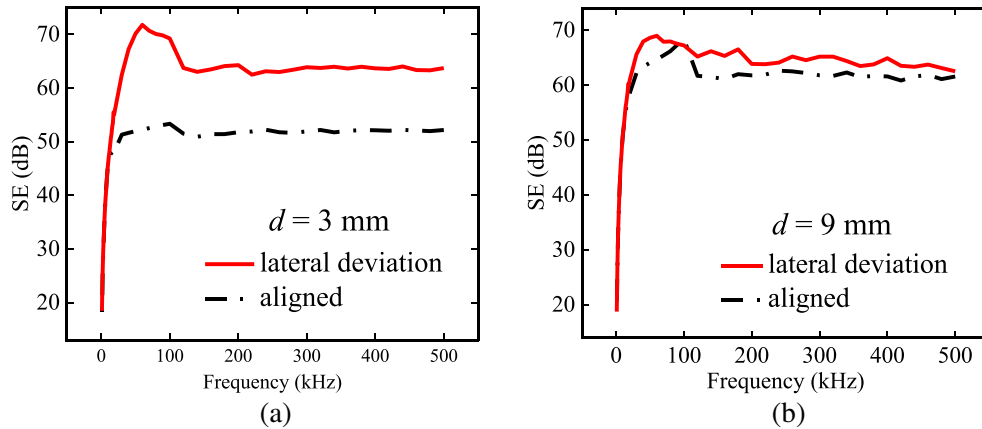
Figure 10. Comparison of SE with and without lateral deviation for a loop-to-loop distance of 92 mm with different layer-to-layer spacings: (a) $d = 3$ mm, (b) $d = 9$ mm.

At a smaller loop-to-loop distance of 69 mm, the influence of lateral deviation on SE is shown in Figure 9. When the loop-to-loop distance is 69 mm, and the layer distance is 0 mm, 6 mm, 9 mm, and 12 mm, the SE increment is approximately 22 dB, 8 dB, 6 dB, and 2 dB, respectively.

The effects of lateral deviation on the SE for loop-to-loop distances of 92 mm and 107 mm are illustrated in Figure 10 and Figure 11, respectively. It is evident that the lateral deviation has no significant effect on the SE when the layer-to-layer spacing d is increased to 9 mm and 6 mm for the loop-to-loop distances of 92 mm and 107 mm, respectively.

According to the results in Figures 8–11, as a conservative estimate, when the layer-to-layer spacing is greater than the aperture diameter, the lateral deviation does not affect the value of the SE.

In the cases discussed above, the aperture diameter is 10 mm. However, the phenomenon still persists even when the aperture diameter is changed. Figure 13 demonstrates the effect of layer-to-layer spacing on SE, taking an aperture diameter of 15 mm as an example. It is evident that there is a rapid increase in SE as the layer-to-layer spacing is increased. In comparison to the close contact case ($d = 0$ mm), the SE increments are approximately 5 dB, 9 dB, and 15 dB for $d = 3$ mm, 6 mm, and 9 mm, respectively.

We also built a finite-size periodic aperture array model in the software CST that was consistent with the experiment [25]. Figure 13 shows the experimental and simulation comparison of the shielding effectiveness versus frequency curve when the spacing is different. Discrete points represent simulation
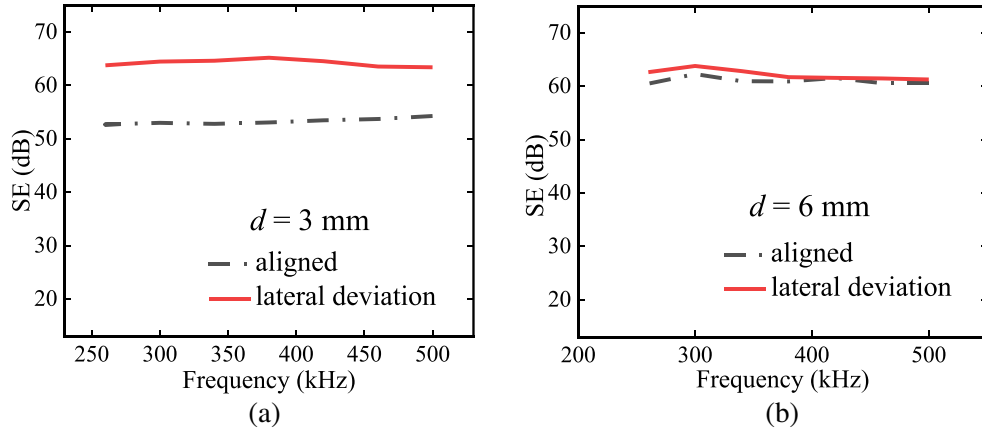
Figure 11. Comparison of SE with and without lateral deviation for a loop-to-loop distance of 107 mm with different layer-to-layer spacings: (a) $d = 3$ mm, (b) $d = 6$ mm.
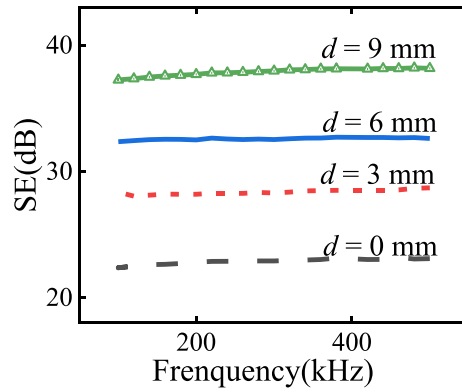

Figure 12. Measured shielding effectiveness versus frequency for different layer-to-layer spacings when the diameter of the aperture is 15 mm.

results, and continuous curves represent experimental test results. As shown below, when $d = 0$ mm, 3 mm, and 6 mm, the results of simulation and experiment are close to each other (3–5 dB), but when $d = 30$ mm, the difference between simulation and experiment is about 8–15 dB. From the results, the consistency between simulation and experiment is not very good. However, there is also a phenomenon that SE increases rapidly with the slight increase of the distance between the two plates.
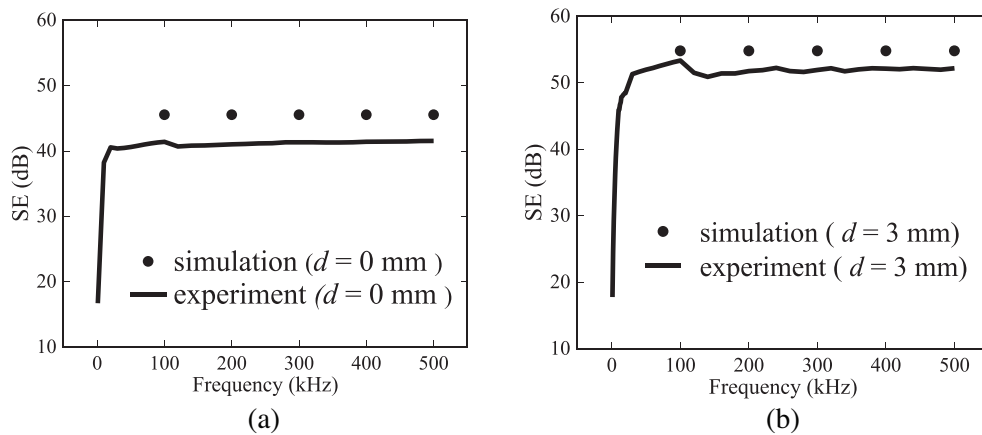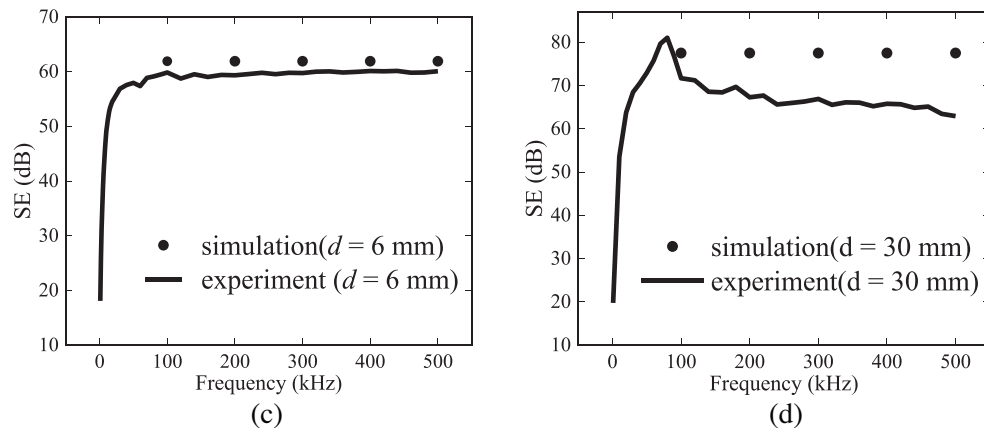
Figure 13. Comparison of simulation and experiment results.

To explain this disagreement, we first state the difference between the practical loop used experimentally and the ideal loop used in the simulated model. The practical loop has a finite wire radius, while the ideal loop has a wire radius of zero. Moreover, the practical loop (especially the emitting loop) has an attached frame structure. This makes it difficult to determine the equivalent radius of the practical loop when it is treated as an equivalent ideal loop. Since both the emitting loop and receiving loop have finite radius and are fixed in a shell with a finite thickness, it perturb the parameters z_1, z, and r_c relative to the original sizes adopted in simulation. The specific original preparation will be determined by future research.

4. CONCLUSION

The experiments conducted aimed to analyze the low-frequency magnetic shielding of double-layer conducting plates with periodic apertures. The following key findings were observed:

1) The SE increases significantly as the layer-to-layer spacing increases from zero to the aperture diameter. For instance, a spacing of 3 mm and 9 mm resulted in SE improvements of 10 dB and 20 dB, respectively.

2) When the layer-to-layer spacing is smaller than the aperture diameter, the lateral deviation between the two layers has a noticeable impact on the SE.

3) When the two plates are stacked together, the surface contact pressure hardly affects the SE.

ACKNOWLEDGMENT

REFERENCES

1. Frikha, A., M. Bensetti, L. Pichon, et al., "Magnetic shielding effectiveness of enclosures in near field at low frequency for automotive applications," *IEEE Trans. Electromagn. Compat.*, Vol. 57, No. 6, 1481–1490, Dec. 2015.

2. Lee, S., D.-H. Kim, Y. Cho, et al., "Low leakage electromagnetic field level and high efficiency using a novel hybrid loop-array design for wireless high power transfer system," *IEEE Trans. Ind. Electron.*, Vol. 66, No. 6, 4356–4367, Jun. 2019.

3. Zhou, Y., L. Zhang, S. Xiu, and W. Hao, "Design and analysis of platform shielding for wireless charging tram," *IEEE Access*, Vol. 7, 129443–129451, Sep. 2019.

4. Zhang, J., T. Lu, W. Zhang, X. Bian, and X. Cui, "Characteristics and influence factors of radiated disturbance induced by IGBT switching," *IEEE Trans. Power Electron.*, Vol. 34, No. 12, 11833–11842, Dec. 2019.

5. Ma, D., M. Ding, J. Lu, et al., "Study of shielding ratio of cylindrical ferrite enclosure withgaps and holes," *IEEE Sens. J.*, Vol. 19, No. 15, 6085–6092, Aug. 2019.

6. Giaccone, L., V. Cirimele, and A. Canova, "Mitigation solutions for the magnetic field produced by MFDC spot welding guns," *IEEE Trans. Electromagn. Compat.*, Vol. 62, No. 1, 83–92, Feb. 2020.

7. Kellogg, J., "Navigating the selection of magnetic resonance imaging shielding systems," *IEEE Trans. Electromagn. Compat.*, Vol. 3, No. 1, 43–46, Mar. 2021.

8. Salvador, K., D. Harmel, L. Oliveira, S. Cabral, and H. Almaguer, "Study of the effectiveness of magnetic shielding for compact power transformers used on mobile applications," *IEEE Latin Am. Trans.*, Vol. 18, No. 6, 1034–1040, Jun. 2020.

9. Frikha, A., M. Bensetti, F. Duval, N. Benjelloun, F. Lafon, and L. Pichon, "A new methodology to predict the magnetic shielding effectiveness of enclosures at low frequency in the near field," *IEEE Trans. Magn.*, Vol. 51, No. 3, 1–4, Mar. 2015.

10. Lovat, G., P. Burghignoli, R. Araneo, E. Stracqualursi, and S. Celozzi, "Closed-form LF magnetic shielding effectiveness of thin planar screens in coplanar loops configuration," *IEEE Trans. Electromagn. Compat.*, Vol. 63, No. 2, 631–635, Apr. 2021.

11. Jiao, C., F. Ning, X. Yang, et al., "Low-frequency magnetic shielding of planar shields: A unified wave impedance formula for the transmission line analogy," *IEEE Trans. Electromagn. Compat.*, Vol. 63, No. 4, 1046–1057, Feb. 17, 2021.

12. Zhang, Z., X. Yang, C. Jiao, Y. Yang, and J. Wang, "Analytical model for low-frequency magnetic field penetration through a circular aperture on a perfect electric conductor plate," *IEEE Trans. Electromagn. Compat.*, Vol. 63, No. 5, 1599–1604, Apr. 6, 2021.

13. Qin, D. and C. Jiao, "Low-frequency magnetic shielding of planar screens: Effects of loop radius and loop-to-loop distance," *IEEE Trans. Electromagn. Compat.*, Vol. 64, No. 2, 367–377, 2022.

14. Park, H. H., "Analytic magnetic shielding effectiveness of multiple long slots on a metal plate using rectangular loops," *IEEE Trans. Electromagn. Compat.*, Vol. 62, No. 5, 1971–1979, Oct. 2020.

15. Bai, W., F. Ning, X. Yang, C. Jiao, and L. Chen, "Low frequency magnetic shielding effectiveness of a conducting plate with periodic apertures," *IEEE Trans. Electromagn. Compat.*, Vol. 63, No. 1, 30–37, Feb. 2021.

16. Criel, S., L. Martens, and D. De Zutter, "Theoretical and experimental near-field characterization of perforated shields," *IEEE Trans. Electromagn. Compat.*, Vol. 36, No. 3, 161–168, Aug. 1994.

17. Araneo, R., G. Lovat, and S. Celozzi, "Shielding effectiveness of periodic screens against finite high-impedance near-field sources," *IEEE Trans. Electromagn. Compat.*, Vol. 53, No. 3, 706–716, Aug. 2011.

18. Sarto, M. S., S. Greco, and A. Tamburrano, "Shielding effectiveness of protective metallic wire meshes: EM modeling and validation," *IEEE Trans. Electromagn. Compat.*, Vol. 56, No. 3, 615–621, Jun. 2014.

19. Hyun, S., I. Jung, I. Hong, C. Jung, E. Kim, and J. Yook, "Modified sheet inductance of wire mesh using effective wire spacing," *IEEE Trans. Electromagn. Compat.*, Vol. 58, No. 3, 911–914, Jun. 2016.

20. Naranjo-Villamil, S., C. Guiffaut, J. Gazave, and A. Reineix, "Lightning-induced magnetic fields inside grid-like shields: An improved formula complemented by a polynomial chaos expansion," *IEEE Trans. Electromagn. Compat.*, Vol. 63, No. 2, 558–570, Apr. 2021.

21. Bai, W., A. Guo, T. Li, R. Cheng, and C. Jiao, "A multi-stage model for the electromagnetic shielding effectiveness prediction of an infinite conductor plane with periodic apertures," *IEEE Access*, Vol. 7, 61896–61903, 2019.

22. Sun, X., B. Wei, Y. Li, and J. Yang, "A new model for analysis of the shielding effectiveness of multilayer infinite metal meshes in a wide frequency range," *IEEE Trans. Electromagn. Compat.*, Vol. 64, No. 1, 102–110, Sep. 1, 2021.

23. Andrieu, G., et al., "Homogenization of composite panels from a near-field magnetic shielding effectiveness measurement," *IEEE Trans. Electromagn. Compat.*, Vol. 54, No. 3, 700–703, Jun. 2012.

24. Yang, X., Z. Zhang, F. Ning, C. Jiao, and L. Chen, "Shielding effectiveness analysis of the conducting spherical shell with a circular aperture against low-frequency magnetic fields," *IEEE Access*, Vol. 8, 79844–79850, 2020.

25. MWS. Framingham, MA, USA, 2015. CST Computer Simulation Technology, 2011. [Online]. Available: http://www.cst.com/Content/Products/MWS/Overview.aspx.